Modelling and Simulation of a Saline Aquifer for CO_2 Injection and Storage

Daniela Carla Moreira de Souza
daniela.souza@ist.utl.pt

Instituto Superior Técnico, Lisboa, Portugal

July 2016

Abstract

A promising method for reducing the impact of the global warming consists in capturing and sequestering the carbon dioxide (CO_2) into geological formations. Deep saline aquifers are great candidates for sequestration once they offer high storage capacities and worldwide distribution. In the present work, a 2D Cartesian model of a Saline aquifer was developed in the gPROMS ModelBuilder, to provide a practical tool to study the feasibility of an aquifer for the CO_2 injection and its dynamic behaviour. The Aquifer model simulates the injection of a specified number of dense-phase CO_2 streams into its injection coordinates. The multiphase flow included the application of Darcy's law extension to each phase (CO_2 and water) and implementation of relative permeability correlations. For validation, the results of simulations of the injection into Johansen formation, obtained the simulator Eclipse E100, were accessed. By applying the formation geological data to specify the developed model, results from simulations of two cases of relative permeability, deviate in only 0.18% and 0.24% from the values predicted by Eclipse, establishing the model validity. Furthermore, to test its applicability and sensitivity to the geological parameters, simulations were performed with sets of subsurface conditions of possible sequestration scenarios around the world, yielding quite realistic results. Lastly, a Case Study of the Transmission and Injection sections of a new state of art power plant at Kingsnorth (UK) retrofitted with Carbon Capture and Storage (CCS) was performed. The simulation was successful and the project design constraints were met..

Keywords: saline aquifer, modelling, multiphase flow, CO_2 injection, gPROMS, CCS

1 Introduction

The highest increase in world-wide energy consumption has been, and will continue to be, associated with fossil fuels: oil, coal and natural gas [1]. Hence the increased interest on mitigation technologies, including the reduction of the energy intensity through efficiency and design improvements, and reduction of the carbon intensity, by switching to lower carbon content fuels such as natural gas. It is unlikely that these methods would be sufficient to meet the commitments undertaken in 1997 Kyoto Protocol, thus, to meet the reduction targets, costlier mitigation approaches need to be considered, foremost among them being Carbon Capture and Storage (CCS) [2].

With the deployment of CCS, the accompanying CO_2 emissions resulting from the continued use of high carbon content fuels, can be sequestered at geological formations, being kept away from the atmosphere for hundreds or thousands of years.

The geological formations considered for sequestration comprise depleted oil and gas reservoirs, deep unmineable coal seams and saline aquifers. Deep saline aquifers are widely distributed around the world and offer large storage volumes. Also, pressure and temperatures regimes on these reservoirs favours the dense-phase injection of CO_2 and they also offer the possibility for enhanced storage through carbonate mineralization on the long term [2].

Hereupon, is possible to recognize that there is a great potential for sequestration of CO_2 into Saline Aquifers. Presently, there are many simulation codes that could be used to model injection of CO_2 into geologic formations. A critical comparison of these codes can be found at [3]. Between the models that were considered, Eclipse 100 and TOUGH2 have been extensively used in the oil and gas industry, the latest being present at the majority of the previous works in the reservoir modelling of CO_2 injection.

Especially concerned with the acceleration of CCS development, its implementation and the management of the associated risk, the ETI CCS System Modelling Toolkit project was launched in 2011. The project aims to create a commercially supported CCS modelling package, that enables the simulation of the operation and design of the whole CCS chain. Between the project participants, PSE represents the modelling expert, supplying the modelling platform, gPROMS advanced process modelling platform, and assisting in the creation of the models and simulation of the operations along the chain ([4]).

Here, a numerical model of a saline aquifer is developed in the gPROMS Model Builder Platform, aiming to simulate the injection of CO_2 into these formations and the accompanying dynamic response. The developed model is validated against results obtained with the commercial simulator Eclipse 100, under comparable conditions. Also, the sensitivity of model to the geological parameters porosity and permeability was studied. Lastly, the model was tested while integrated in a flowsheet, with models that belongs to the gCCS modelling Toolkit library. With this flowsheet assembly, a dynamic study of the operation the operation of the Transport/Injection Chain was conducted.

2 Background

The final stage of a CCS chain consists in the CO_2 injection into deep underground rock formations. The seal or cap-rock, an impermeable rock that exists on the top of these formations, and the trapping mechanisms prevent the CO_2 from returning to the surface.

The density of the CO_2 will increase with depth. At depths of about 800 m or greater, it will be in a dense supercritical state. The temperature and pressure keep the CO_2 in a liquid-like density that enhances the efficiency of the utilization of underground storage [5].

When CO_2 is injected into a saline aquifer, it displaces saline formation water and then migrates buoyantly upwards. After injection, the with CO_2 can remain trapped underground by of a number of mechanisms, such as: trapping the under the cap-rock; retention as an immobile phase trapped in the pore spaces of the storage formation; dissolution in the in situ formation fluids; and/or adsorption into organic matter in coal and shale. Ultimately, CO_2 becomes less mobile over time as a result of the trapping mechanisms, further lowering the prospect of leakage and increasing the storage security (Figure 2.1).

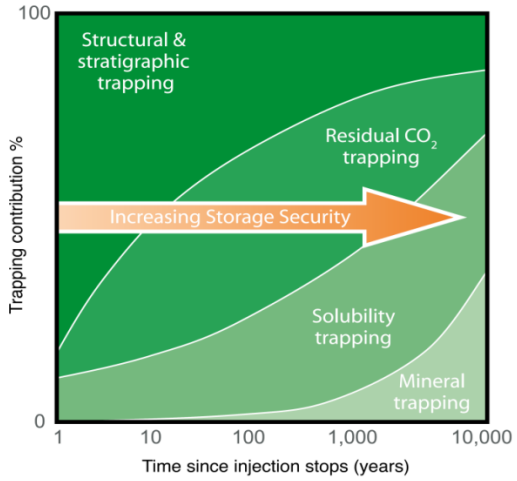

Figure 2.1 – Trapping mechanism and storage security (after [5])

2.1 Reservoir rock characteristics

The properties of the sedimentary rocks govern their physical and chemical properties, hence the fate of the carbon dioxide stored in them.

The majority of rock and soils contains a certain percentage of empty spaces which may be occupied by fluids (liquids and/or gases). The ratio between the volume not occupied by solid framework and its bulk volume is recognized as porosity, $\emptyset$:

$$\emptyset = \frac{V_p}{V_b} \qquad 2.1$$

V_p (m^3) stands for the porous volume and V_b (m^3),for the bulk volume of the rock.

The aquifer permeability measures its capacity and ability to transmit fluids. It can only be defined together with the fluid flow, by means of the Darcy's law [6]. For a simple case of a horizontally oriented rock core subjected to a pressure gradient, the mass flowrate of a fluid, F (kg/s), will be given by:

$$F = -kA\frac{\rho}{\mu}\frac{dP}{dx} \qquad (2.2)$$

A (m^2) represents the cross section perpendicular to the flow, μ $(Pa.s)$ and $\rho(kg/m^3)$ the viscosity and mass density of the fluid occupying the porous space, respectively. $k(m^2)$ is the intrinsic permeability of the rock, defined when the porous media is completely saturated with one fluid.

In the multiphase flow in the subsurface, different phases exist and occupy the medium pore space at the same time. For a given phase β, the presence of others reduces the flow path. The fractional flow of each fluid is thereby determined by its relative permeability, $k_{r_\beta}(-)$, a measure of the ability of the porous system to conduct one fluid when more than one fluid phase occupy the porous media. The effective permeability of the phase β comes:

$$k_\beta = k_{r_\beta} \times k \qquad (2.3)$$

The multiphase extension of Darcy's law defines the flow velocity, $\overrightarrow{u_\beta}(m/s)$:

$$\overrightarrow{u_\beta} = -k\frac{k_{r\beta}}{\mu_\beta}\left(\vec{\nabla}p_\beta - \rho_\beta\vec{g}\right) \qquad (2.4)$$

These flow properties are the composite effect of pore geometry, wettability, fluid distribution, and the fluid saturation of a generic phase β, S_β, i.e. the ratio between the pore volume occupied by the phase and the pore volume available for flow [7].

There are a number of two phase characteristic curves relating capillary pressure and phase saturation to solve for capillary pressure and relative permeability numerically from two-phase flow experiments. From these characteristic curves, Brooks and Corey [8] and van Genuchten [9] are the most widely assumed in reservoir simulations, being implemented at the developed model.

3 Mathematical model

The injection of CO_2 involves the simultaneous flow of the CO_2 and the brine in the porous medium. The fundamental principle behind the flow description is the conservation of mass. The main physical mechanisms that can come into play in the transport are convection, diffusion and dispersion.

By reviewing the CO_2 trapping mechanisms and their impact on the storage security (Figure 2.1), it can be grasped that the Structural and Stratigraphic trapping and the Residual trapping are the main mechanisms responsible for the CO_2 sequestration for the timescale of interest for the CCS. Thus, the effect of chemical reactions and adsorption will not be included in the considered model.

Two fluid phases considered are an aqueous or water-rich phase, referred to as liquid-phase and a single CO_2-rich phase, referred to as gas-phase. Therefore, the flow mechanism of transport will consist on the multiphase immiscible flow of the liquid- and gas-phases in the porous media, being governed by convection.

The approach followed to model the proposed saline aquifer reservoir is in conformance with the formulation of the simulator TOUGH2 [10].

3.1 Governing equations

For an arbitrary volume V_n of the porous medium bounded by a surface Γ_n, the rate at which the mass of phase β changes in V_n is balanced by its net inflow by convection, and the inflow and outflow arising from injection and extraction processes, respectively. The mass of phase β contained in a differential element of volume dV_n, $M_\beta(kg)$, will be expressed by:

$$dM_\beta = \phi \rho_\beta S_\beta dV_n \tag{3.1}$$

Part of the accumulation of phase β in dV_n is due to its transport in and out of the control volume boundaries. At any differential element of area $d\Gamma$, the convective flux of phase β, $\overrightarrow{J_\beta}(kg/m^2 s)$, is given by:

$$\overrightarrow{J_\beta} = \rho_\beta \overrightarrow{u_\beta} \tag{3.2}$$

The injection and extraction terms describe the flow of fluids into and out of the aquifer. These terms are modelled as if there were a creation or disappearance of mass of the differential element of volume dV_n, i.e. as a source and a sink terms ($Q_\beta(kg/m^3)$). The integral material balance for the phase β comes:

$$\frac{d}{dt}\int_{V_n} M_\beta dV_n = -\int_{\Gamma_n} \overrightarrow{J_\beta}.\vec{n} d\Gamma_n + \int_{V_n}\left(Q_{\beta_{injected}} - Q_{\beta_{extracted}}\right) dV_n \tag{3.3}$$

To understand the spatial distribution of phase β, the continuity equation was derived, by applying the Reynolds Theorem to the equation (3.3) and assuming a stationary volume of control. Lastly, the final form of the continuity equation, applied at this model implementation, is obtained:

$$\frac{\partial M_\beta}{\partial t} = \frac{1}{V_n}\sum_m j_{\beta_{nm}} A_{nm} + F_{\beta_{injected}} - F_{\beta_{extracted}} \tag{3.4}$$

3.2 Model Implementation

Equation (3.4) is used as the starting point to derive the finite differences, with the integral finite difference (IFD) method by Narasimhan and Witherspoon being employed to discretize the mass balance [11]. The gPROMS ModelBuilder is used for the implementation of the model and the accumulation of mass will be evaluated recurring to the explicit time derivatives.

One important assumption is the homogeneity of the reservoir. The permeability will be, by default, equal in the x and y-direction of flow. Once the aquifer thickness will be quite small compared to its extension in the x- and y-directions, the pressure gradient in the z-direction will be neglected, i.e. vertical equilibrium.

In gPROMS notation, the discrete element variables will be represented as an array with the position given by the indexes (i,j). The continuity equation was implemented for each element of the defined grid:

$$\frac{\partial M_{\beta\ PUV_{(i,j)}}}{\partial t} V_{(i,j)} = j_{xx_{\beta\,(i,j)}} A_{x(i,j)} - j_{xx_{\beta\,(i+1,j)}} A_{x(i+1,j)} + j_{yy_{\beta\,(i,j)}} A_{y(i,j)} - j_{yy_{\beta\,(i,j+1)}} A_{y(i,j+1)} + F_{\beta_{injection_{(i,j)}}} - F_{\beta_{extraction_{(i,j)}}} \tag{3.5}$$

with (i,j) representing the evaluated discrete element x and y coordinates. The balances are performed for all discrete elements. The same notation will be used in the following equations. The flux terms will be defined in each interface between consecutive grid elements. For the x-direction of flow:

$$j_{xx_{\beta(i,j)}} = -k_{xx(i-1,j)} \frac{k_{r\beta\,xx_{(i-1,j)}} \rho_{xx_{\beta(i-1,j)}}}{\mu_{\beta\,xx_{(i-1,j)}}} \left(\frac{p_{\beta_{(i,j)}} - p_{\beta_{(i-1,j)}}}{(dx_i + dx_{i-1})/2}\right) \tag{3.6}$$

The holdup variables relation to the volume of porous media, and the fluid phase density will be given by the following equations:

$$M_{\beta\ PUV_{(i,j)}} = \phi_{(i,j)} S_{\beta_{(i,j)}} \rho_{\beta_{(i,j)}} \tag{3.7}$$

$$M_{\beta_{(i,j)}} = M_{\beta\ PUV_{(i,j)}} V_{(i,j)} \tag{3.8}$$

$$V_{\beta_{(i,j)}} = \frac{M_{\beta_{(i,j)}}}{\rho_{\beta_{(i,j)}}} \tag{3.9}$$

$$\sum_{i=1}^{N_x}\sum_{j=1}^{N_y} S_{\beta_{(i,j)}} = 1 \tag{3.10}$$

To evaluate the relative permeability, Brooks and Corey and van Genuchten correlations were implemented ([8], [9]). No-flow boundary conditions are applied and, for the physical properties calculation, the Multiflash foreign object, literature correlations and extrapolation of existing data methods were made available.

To calculate the average properties between consecutive grid elements, the upstream weighting scheme will be employed. In the x-direction, they are implemented for the density, ρ_{xx}, permeability, k_{xx}, relative permeability, $k_{r_{xx}}$, and viscosity, μ_{xx}. The first and last coordinates of the boundaries of the elements of the grid will be defined by the reservoir dimensions and the interfacial areas, normal to the flow, will be given by:

$$A_{x(j)} = dy_j dz \tag{3.11}$$

$$A_{y_{(i)}} = dx_i dz \tag{3.12}$$

By default, the grid elements will be equally spaced but the model can also accommodate proper user defined grid refinements. A degree of freedom analysis showed that the following specifications are required:

- Inlet streams conditions (T, F, w)

The variables to be assigned initial values will be:

- Initial pressure of reservoir;
- Initial volume saturation of liquid-phase.

4 Validation and Sensitivity analysis

4.1 Model validation

For model validation, simulations were performed, with a set of petrophysical properties of the Johansen formation. Eigestad et al. developed a geological model of this

formation, based on available seismic and well data [12]. In addition, simulations of the injection into Johansen were performed using the industry standard black oil simulator Eclipse 100. Using the Eclipse results as an evaluation basis, the developed model was tested under a comparable injection scenario.

In Figure 4.1, the relative permeability curves predicted by the van Genuchten correlations, are plotted against the original curves obtained from the Johansen dataset. The van Genuchten parameter, m, related to the pore distribution, was tuned for each phase. A large discrepancy between the curve is observed for the entire range of liquid saturations.

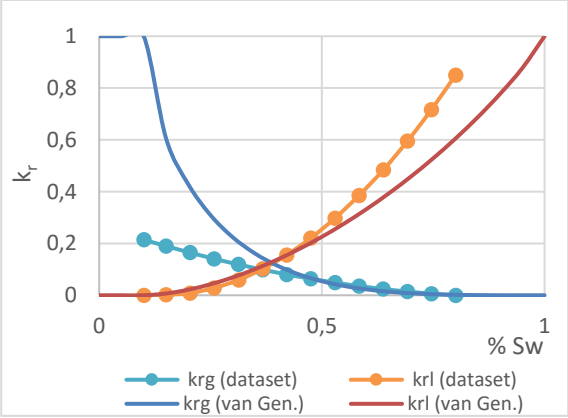

Figure 4.1 – Original kr curves (after [12]) and adjusted van Genuchten correlation (m_{gas} = 1.5 and m_{liquid} = 0.85)

Corey correlation was also studied and, once more a parameter fitting was performed. The respective curves show a higher degree of consistency than the van Genuchten for the liquid-phase. In fact, it can be seen that the liquid-phase curve shows a very good degree of consistency (Figure 4.2).

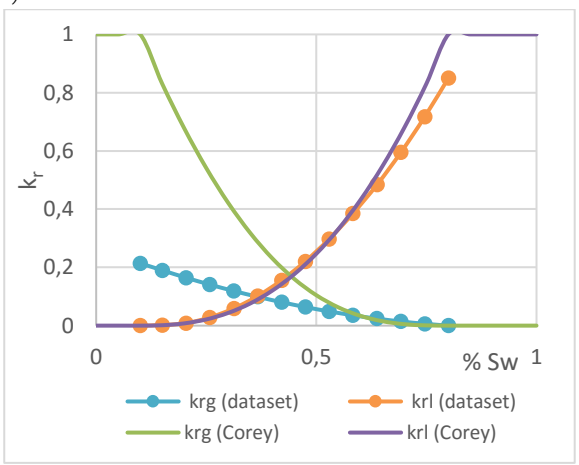

Figure 4.2 – Original kr curves (after [12]) and adjusted Corey correlation (n_{gas} = n_{liquid} = 2.5)

Different combinations of relative permeability correlations were employed in the simulations. Case 1 and 2 study the injection with Corey and van Genuchten correlations, respectively. Case 2 employ Corey correlation for the gas- and van Genuchten liquid-phase saturation. Lastly, Case 4 utilize van Genuchten gas-phase saturation and Corey correlation for the liquid. for the liquid correlation. for relative permeability calculation.

Further, there were some characteristics of the Johansen Geological model simulations that were directly assigned to the Saline Aquifer included injection flowrate, temperature and the irreducible saturations (Table 4.1).

Table 4.1 – Johansen formation injection characteristics

Characteristic	**Value (after [13])**
Injection Flowrate	3.5 Mton/year
Temperature	Constant (94 ºC)
Irreducible water saturation	0.1
Irreducible CO_2 saturation	0.2

The Lookup interpolation method featured on gPROMS Model Builder was utilized to read the fluid system the data-file comprehended at the Johansen Data set. The data filet characterizes an immiscible, two-phase isothermal system of water and CO_2 phases. The densities and viscosities were given for 94 ºC and pressure values in the range that exists during the simulation time, (from 230 to 400 bar). Table 4.2 summarizes the specifications of the saline aquifer model employed at the Johansen formation simulations.

Table 4.2 – Johansen formation study petrophysical properties and geometry specifications

Characteristic	**Value**
Initial pressure	306 bar
Reservoir thickness	Uniform (100 m)
Lateral extensions	60 x 100 km
Flow geometry	2D (x-y)
Grid characterization	$N_x = N_y$ = 101elements
Grid refinement	None
Permeability	Isotropic (500 mD)
Porosity	0.25

Johansen Formation simulations results

The wellblock pressure obtained from the simulations of the injection into Johansen, performed with the developed model, are presented on Figure 4.3. It's important to pinpoint the fact that, on the results presented henceforth, the number of grid elements was limited to 101 in each direction, due to computational constraints.

Confronting the results with the ones obtained with Eclipse [13], it can be noticed that the first transient response and the second phase of increase were respectively not as sharp and sluggish. Nevertheless, by the end of 80 years of injection, the wellblock pressure predicted by the Cases 1 and 4, where Brooks and Corey correlation was used in the description of the liquid relative permeability, have fallen over the same range anticipated by the Eclipse simulations. In fact, for these cases, the final result deviates in only 0.18% and 0.24%, respectively, from the values predicted by the detailed geological model with the no-flow boundaries condition, Table 4.3.

Table 4.3 – Final pressures attained at Johansen Injection and deviation from Eclipse results

	Case 1	Case 2	Case 3	Case 4
Pressure(bar) $_{80\ years}$	317,39	323,37	322,52	317,57
Deviation from Eclipse results$_{80\ years}$ No flow boundaries	0,18%	2,07%	1,81%	0,24%

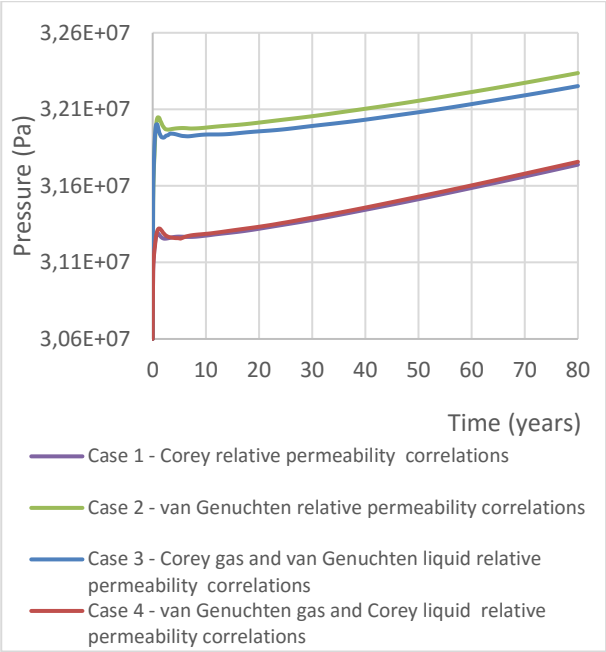

Figure 4.3 – Johansen aquifer wellblock pressure for different sets of relative permeability correlations

Corey formulation is the correlation with a better fit to the Johansen original permeability, being the reason behind the large difference between the wellblock pressure and demonstrating the importance of the relative permeability description.

The pressure buildup is highly dependent on relative permeability representation. Additionally, the grid refinement also plays an important part, particularly on the accuracy of the results and capture of the transient response on the first five years of injection. The effect of the number of grid elements on the pressure build-up was investigated. Figure 4.4 shows the effect of the grid refinement on the pressure response for the Case 1.

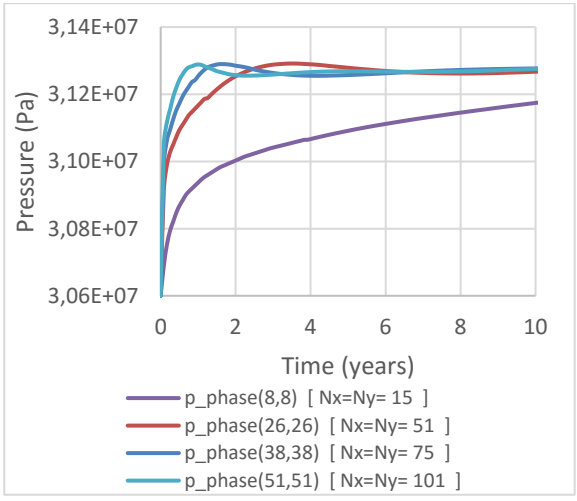

Figure 4.4 – Johansen aquifer grid effect on wellblock pressure analysis for Case 1

With the grid effect analysis, it was possible to see that the initial wellblock pressure response was as fast and prominent as larger the number of grid elements evaluated. To study this outcome, the mass fluxes were evaluated in the x-direction taking the east face of the wellblock and the N_x= N_y=101 and N_x= N_y=51 grid cases (Figure 4.5). The gas-phase was nearly immobile in the early beginning when, in parallel, the liquid was rapidly pushed out of the wellblock. The grid refinement ruled the length of the initial period, once there was a delay on the response of approximately two years.

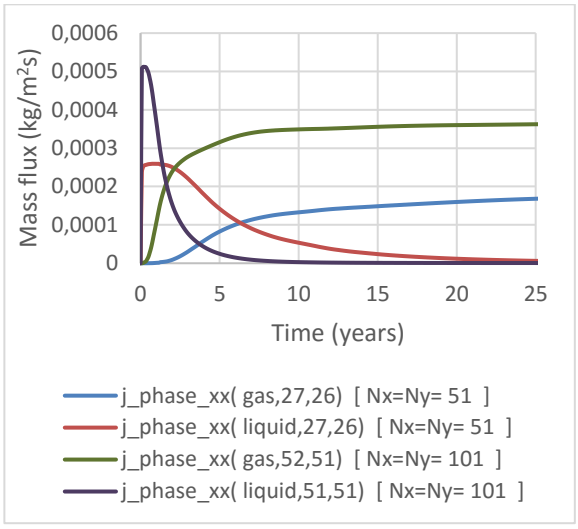

Figure 4.5 – Johansen aquifer mass fluxes at the east face of wellblock analysis for Case 1

The volume saturation dependant relative permeability grounds the mass fluxes behaviour (Figure 4.6). Before the injection begins, the gas-phase is only found in the residual form in the aquifer. Accordingly, its low relative permeability will hinder its movement while the wellblock liquid-phase relative permeability assumes its maximum value, explaining the instantaneous movement of the liquid-phase.

The CO_2 accumulation in the wellblock aids the gas-phase saturation growth and, accordingly, its relative permeability, launching the CO_2 movement to the surrounding grid elements. The combination of increasing relative permeability and installed pressure gradient between the wellblock and surrounding grid elements underlies the small decrease in the pressure.

In the long term, all the simulations performed with different number of discrete elements have given rise to coherent results that fall into the same range of the ones obtained with Eclipse. Therefore, among the fundamental differences between the models, the difference between the initial responses are essentially governed by the grid refinement effects. Nevertheless, the curve shapes and the long term convergence demonstrate a fair degree of consistency between both models.

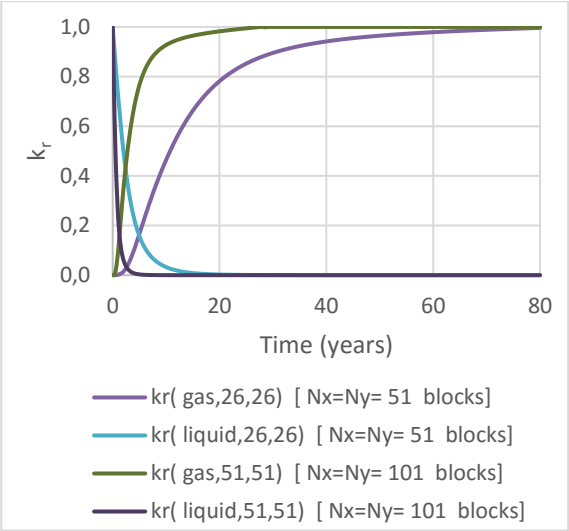

Figure 4.6 – Johansen aquifer wellblock relative permeabilities analysis for Case 1

A final look will be given to the pressure distribution at the aquifer (Figure 4.7 and Figure 4.8).

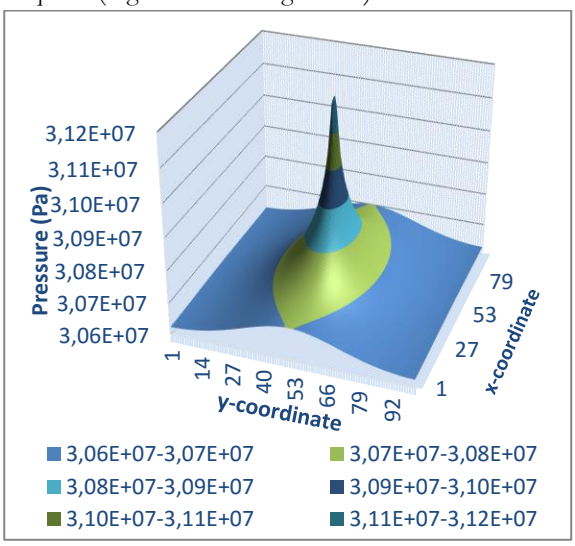

Figure 4.7 – Pressure distribution in the Johansen formation after 10 years of injection for Case 1

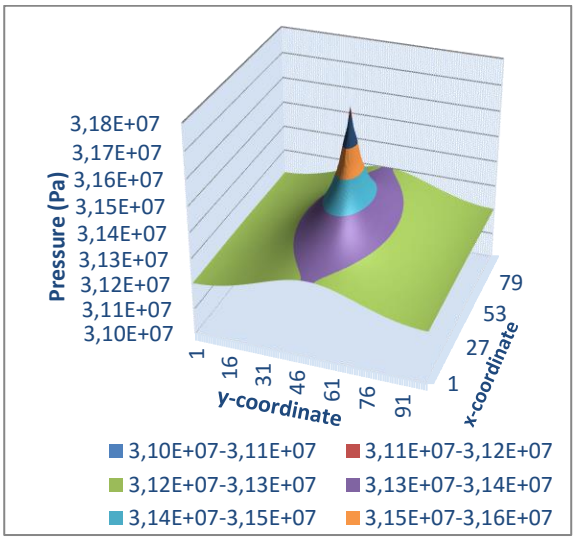

Figure 4.8 – Pressure distribution in the Johansen formation after 80 years of injection for Case 1

At the end of 10 years, the pressure perturbation caused by the CO_2 injection is mainly focused in the near wellblock area and the cone shaped pressure distribution is slightly distorted in the x-direction, showing a faster disturbance spread. This trend is observed because the Johansen aquifer dimensions are distinct. After 80 years, the whole reservoir extension has been affected by the CO_2 injection, with an increase of 6 bar at the y-direction boundaries, the furthest away from the wellblock.

4.2 Model applicability and sensitivity analysis

The petrophysical properties of the reservoir heavily affect the flow characteristics, hence the CO_2 and pressure distributions. Thus, in this subsection, a sensitivity analysis will be performed to the main parameters that influence it, namely the permeability and porosity. The basic model specifications required to perform the sensitivity analysis simulations were grounded on earlier studies of CO_2 injection modelling ([14], [15]), being summarized in Table 4.4 and Table 4.5.

Table 4.4 – Sensitivity analysis simulations specifications

Property	Value	
Physical properties	Multiflash	
Injection time	30 years	
Initial pressure	120 bar	
Temperature	Reservoir	45ºC
	CO_2 stream	
Injection flowrate	100	
Relative permeability correlation	van Genuchten	
	S_{lr}=0.30	
	S_{gr}=0.05	
	m=0.46	

Table 4.5 – Sensitivity analysis grid configuration

Variable	Value
Grid configuration	$N_x = N_y$= 75 elements
	N_{wells}= 1 well
	$x_{well} = y_{well}$= 38
Extension in x and y directions	100 km

To establish the range over which the petrophysical properties vary, basins suitable for CO_2 sequestration were investigated [5]. The porosity and permeability sensitivity analysis simulation settings are displayed on Table 4.6 and Table 4.7, respectively.

Table 4.6 – Porosity sensitivity analysis simulations settings

Variable	Value	Unity
Intrinsic permeability	500	mD
Porosity	0.12 / 0.2 / 0.25 / 0.3 / 0.35	-

Table 4.7 – Permeability sensitivity analysis simulations settings

Variable	Value	Unity
Intrinsic permeability	50 / 500 / 5000	mD
Porosity	0.25	-

Porosity sensitivity analysis

The pressure on the grid element that encloses the injection/well term (wellblock), obtained for the porosity sensitivity analysis cases simulations are depicted in Figure 4.9. For the first 5 years, the wellblock pressure showed a similar development trend, with little dependence on the porosity for all the cases studied. Nevertheless, after this first period, the wellblock pressure starts to diverge with a rate of growth inversely proportional to the studied porosity values.

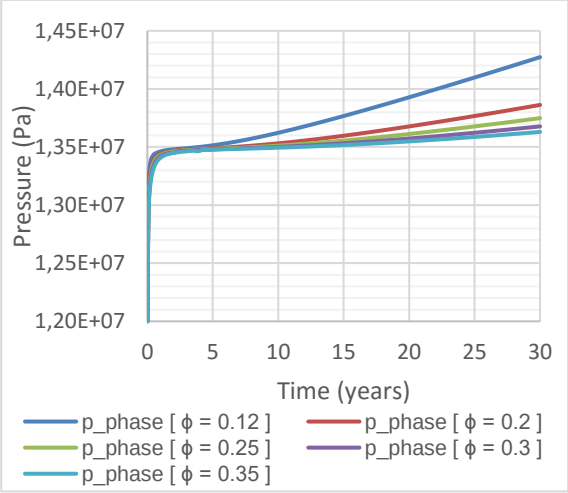

Figure 4.9 – Wellblock pressure for porosity sensitivity analysis

For all the studied cases, a pressure increase of about 12% was seen at the end of the first year. A second period of growth followed, with a pressure rise far more distinct between the cases. For the smaller porosity studied (ϕ = 0.12), an increase of 6.0% was seen when, for the higher porosity case (ϕ = 0.35), the increase was significantly smaller, only 1.6%. To assess the perturbation spread, the pressure distribution was evaluated in the x-direction at the end of 5, 10, 20 and 30 years of injection for both extreme cases.

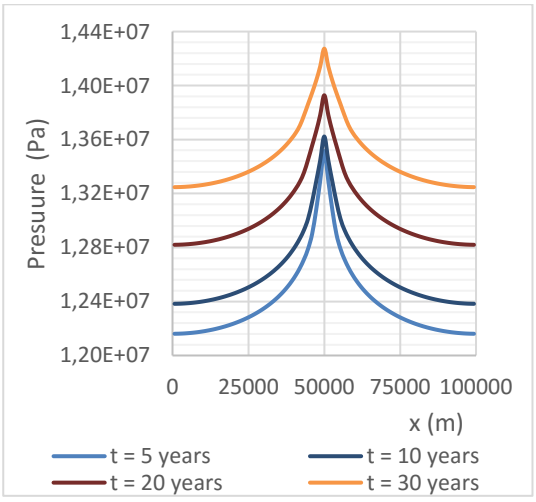

Figure 4.10 – Pressure distribution for ϕ = 0.12

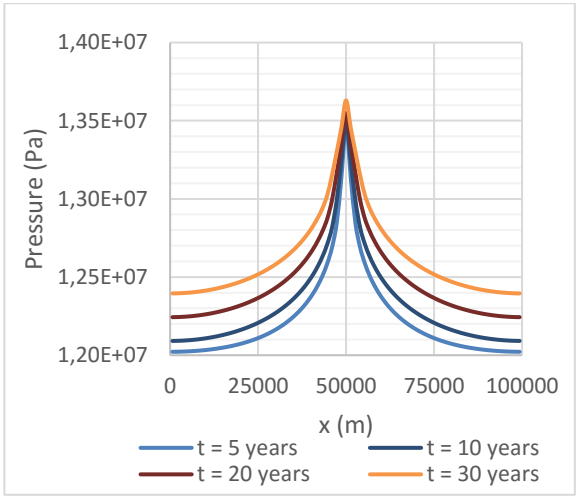

Figure 4.11 – Pressure distribution for ϕ = 0.35

The pressure distributions highlighted the fact that, for the smaller porosity case, the pressure perturbation was quickly transmitted to the whole aquifer extent. The porosity is an indicator of the reservoir capacity and once the permeabilities are held constant, to maintain the continuous injection, the pressure has to increase much more significantly, in order to push and compress the resident brine. Hence the global pressure increase that is immediately seen.

Permeability Sensitivity analysis

The wellblock pressure obtained for the permeability sensitivity analysis is showed on Figure 4.12.. Unlike what was seen for the porosity (Figure 4.9), there is a large difference between the results, not only in value but also on the development trends. Two periods of growth were detected with opposite dependencies on the permeability.

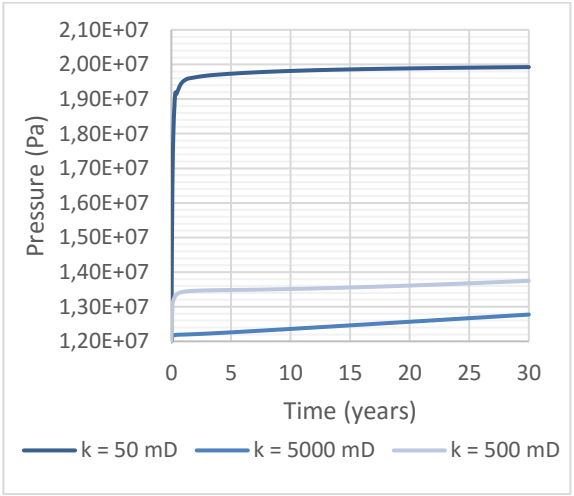

Figure 4.12 - Wellblock pressure for permeability sensitivity analysis

An abrupt rise is seen at the beginning of injection, by the end of the first year with growths of 66%, 15% and 6% identified for the 50 mD, 500 mD and 5000 mD cases, respectively, showing rates of growth inversely proportional to the permeability. Inversely, at the years that follow, an increase of 2% is observed for the smallest permeability case (50 mD), 2.3% for the intermediate (500 mD) and 4.7% for the highest (5000 mD).

To evaluate the permeability effect on the global reservoir extension and on the different rates of growth referred above, the pressure distribution in the x-direction was assessed after 5, 10, 20 and 30 years of injection cases.

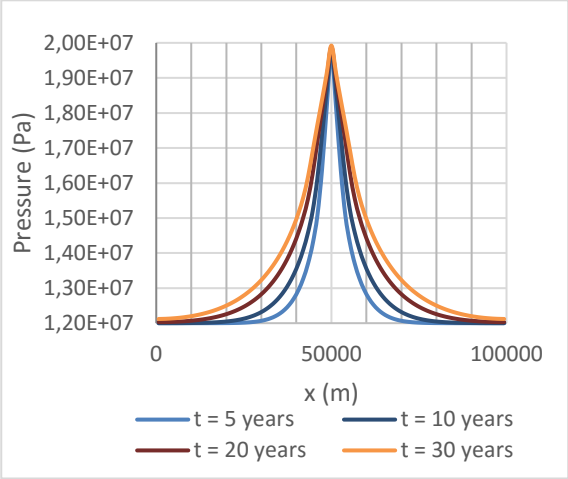

Figure 4.13 – Pressure distribution for k = 50 mD

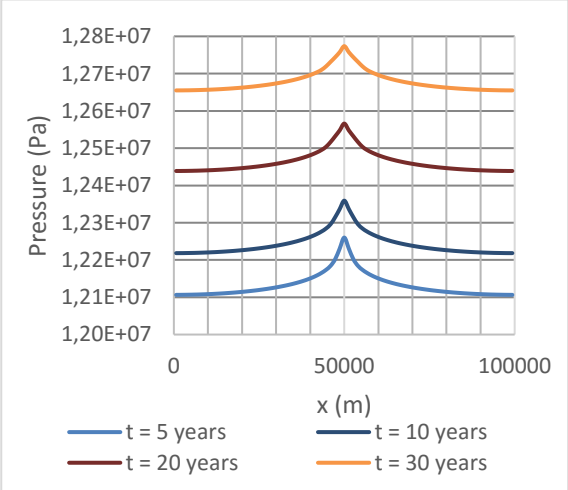

Figure 4.14 – Pressure distribution for k = 5000 mD

The sharpest pressure profile was seen for the lowest permeability case (50 mD) (Figure 4.13), and the perturbation advanced towards the neighbouring grid elements with a simultaneous expansion of the perturbed area. Yet, no major pressure rises were detected at the aquifer borders and wellblock. The perturbation rapidly travelled throughout the aquifer for the 5000 mD case (Figure 4.14), triggering a global pressure increase.

5 Modelling a CCS transportation and storage chain

The injection chain of the Kingsnorth Carbon Capture & Storage Project is hereby studied, by employing the models comprised in the gCCS libraries and the developed model of a saline aquifer. The scope focuses on the confrontation of the planned Full-flow injection flowrate (26400 tonnes/day) against the facility design constraints.

A complete overview of the project details, including the equipment design conditions can be found at the project documentation ([16], [17]).

5.1 Case Study Implementation

The implementation was done in accordance with the Process Flowsheet Diagram (PFD) of the Offshore & Transport System for the Base Case [18] resorting to gCCS Transportation, and gCCS Injection and Storage libraries models. The developed model of a Saline Aquifer was also included at the flowsheet as the final destination of the captured CO_2. The flowsheet was divided in two sections):

- Transportation: main onshore and offshore pipelines;
- Injection/Storage: well system and reservoir.

To specify the models comprised at the flowsheet, the documentation related to the Kingsnorth project was used ([18], [19]). The aquifer model specification to the case study can be found at Table 5.1.

Table 5.1 – Saline Aquifer specifications for the Case Study simulation

Physical properties Calculation	Multiflash
Injection time	10 years
Relative permeability correlation	van Genuchten
	S_{lr}=0.30
	S_{gr}=0.05
	m=0.46
Extension in x and y directions	100 km
Grid dimension:	$101\ x\ 101$ elements

The simulation time was set to 10 years in order to estimate the dynamic behaviour of the system without compromising the computational time.

5.2 Simulation results

The figures presented henceforth illustrate the initial results and the ones obtained at the 1st, 2nd, 3rd, 5th, 7th and 10th years of simulation, with the objective of illustrating the gradual development of the properties profiles results, at the equipment that constitute the injection and storage flowsheet studied.

An evaluation of the results obtained for the equipment that present the greatest interest in the Case Study, the pipelines and the aquifer model, is hereby introduced.

Onshore pipeline results

The onshore pipeline pressure profile holds its initial shape throughout the years, with a global increase of pressure taking place over its entire length, Figure 5.1. At the end of the first year of injection, there is a strong upsurge of the pressure and, afterwards, an almost steady rate of growth is observed.

Although there is a large range over which the pressure varies, the design conditions of 150 barg [16] are secured. The onshore pipeline temperature distribution showed no major variations and the pipeline design conditions were fulfilled. Moreover, the density distribution showed that the CO_2 flows at dense-phase, as a supercritical fluid.

A fast initial pressure increase was seen both upstream and downstream the pipeline, being related to the start-up of

the injection and the accompanying reservoir pressure response.

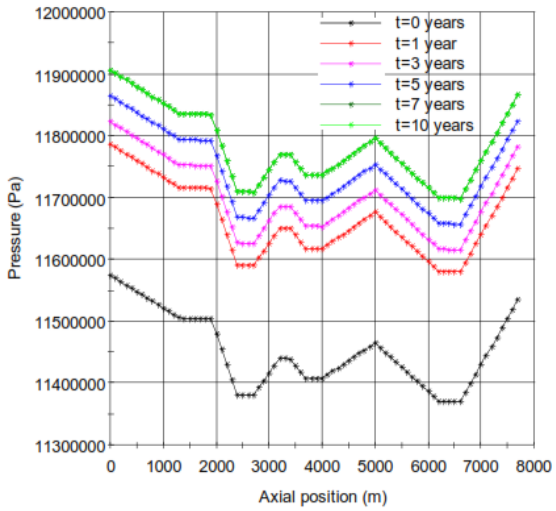

Figure 5.1 – Onshore pipeline pressure distribution

Offshore pipeline results

The offshore pipeline pressure distribution is showed at Figure 5.2. A similar behaviour to the onshore pipeline is observed.

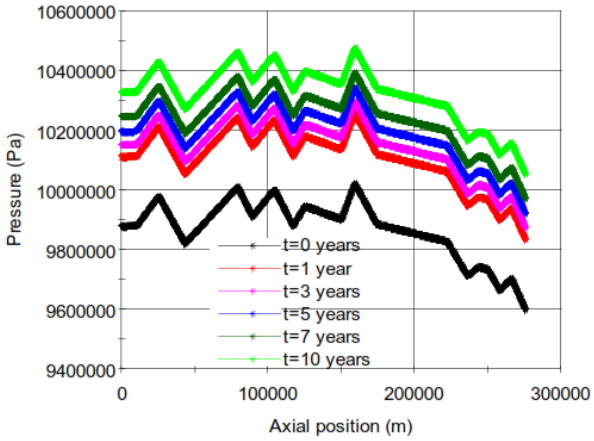

Figure 5.2 – Offshore pipeline pressure distribution

The offshore pipeline temperature distribution does not display major changes throughout the 10 years of simulation, and a substantial temperature decline takes place at its entry. This happens due to the heat transfer between the flowing CO_2 and the surroundings, the cold seabed water.

Saline Aquifer results

The well configuration was chosen to minimize their interaction. This expected interaction is seen here, as illustrated by representation of the inlet pressure at each injection point (Figure 5.3).

In response of the observed difference in pressure development at each wellblock, the inlet mass flow rates diverge, Figure 5.4. For the purpose of monitoring the pressure distribution at the aquifer, its representation after the 1st year of injection is shown on Figure 5.5. Once the initial reservoir pressure was set to 158 bar, at this time, the response to the injection is mainly felt at the well coordinates and surrounding grid elements at first, with a smaller pressure increase being felt at the points further apart from the well coordinates.

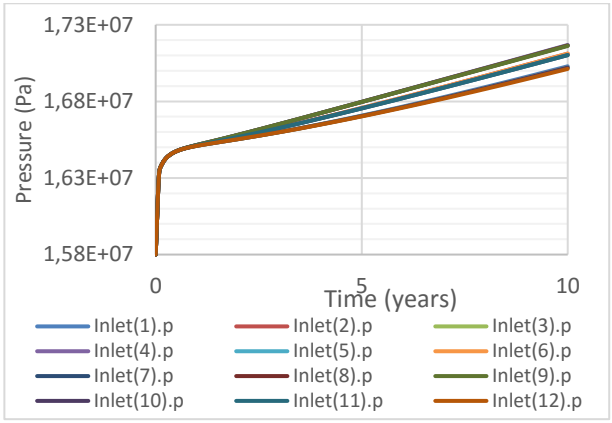

Figure 5.3 – Saline Aquifer inlet pressures

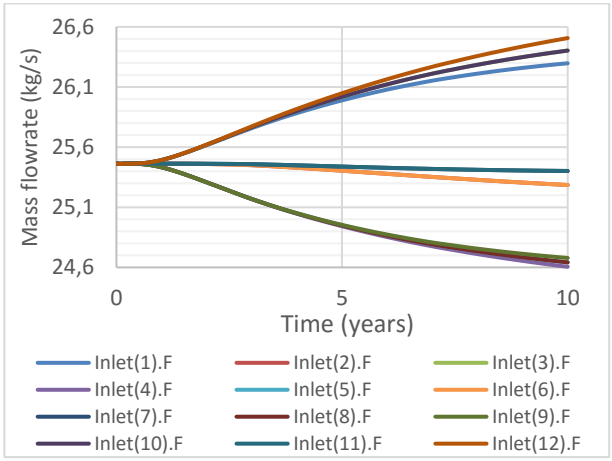

Figure 5.4 – Saline Aquifer inlets mass flow rates

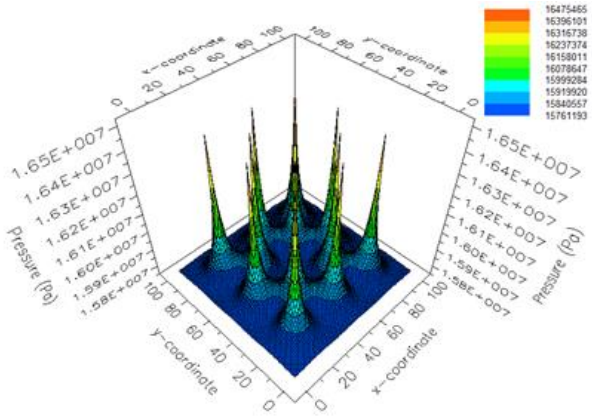

Figure 5.5 – Saline Aquifer pressure distribution for t=1 year

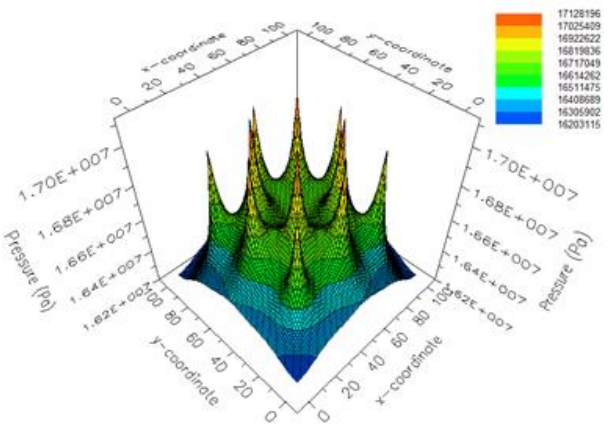

Figure 5.6 – Saline Aquifer pressure distribution for t = 10 years

6 Conclusions

On the present work, a model of a Saline Aquifer was developed, meeting the objective of foreseeing the effect of the CO_2 sequestration on the existing pressure regimes of these geological formations. The model demonstrated a good compromise between simplicity and performance.

The developed model was evaluated, by simulating the injection into the Johansen formation. The pressure development trends were comparable, falling in the same range as predicted by the Eclipse simulations of the same problem. The initial transient response to the injection of CO_2, however, were much less marked. It is believed that the grid refinement is the key player on the accuracy of the results and capture of the transient response on the injection early years. By the end of 80 years, for the simulations where Corey correlation was used to describe the relative permeability of the liquid phase, Cases 1 and 4, the final result deviates only 0.18% and 0,24%, respectively, from the value predicted by the detailed geological model with no-flow boundaries condition.

The porosity sensitivity analysis gave rise to wellblock pressures with a rate of growth inversely proportional to the studied porosity values. Also, this study showed that the velocity of propagation of the disturbance set by the injection of CO_2, is as high as the smaller the porosity of an aquifer. As for the permeability sensitivity analysis, differences on the pressure profiles and the expansion of the perturbed area are very substantial. For higher permeabilities, flatter pressure profiles are seen, as a result of the quick perturbation spread and, for higher permeability cases, piercing pressure profiles are attained but no major pressure buildup take place at the aquifer borders.

To finish the study, the aquifer model was successfully evaluated within a test study of the Transmission and Injection sections of a new state of art coal fire power plant at Kingsnorth retrofitted with CCS. The design constraints of the equipment included at the flowsheet, were met.

7 Bibliography

[1] IEA, "International Energy Outlook 2007," Energy Information Administration, Washington, DC, 2007.

[2] H. Herzog, E. Drake and E. Adams, "CO2 capture, reuse, and storage technologies for mitigating global climate change," Massachussets Institute of Technology, Cambridge, MA, 1997.

[3] H. Class, A. Ebigbo, R. Helmig, H. K. Dahle and J. M. Nordbotten, "A benchmark study on problems related to CO2 storage in geologic formations," *Computational Geosciences,* pp. 409-434, 12 August 2008.

[4] Costas Pantelides, Process Systems Enterprise, *CCS System Modelling Tool-kit Project,* 2012.

[5] Jason Anderson et al., "IPCC Special Report on Carbon dioxide Capture and Storage: Underground Geological Storage," Cambridge University Press, New York, NY, 2005.

[6] G. de Marsily, Quantitative hydrogeology, Orlando, Florida: Academic Press,, 1986.

[7] J. Forrest F. Craig, The Reservoir Aspects of Waterflooding, New York: Millet the printer, 1971.

[8] R. H. Brooks and A. T. Corey, "Hydraulic Properties of Porous Media," *Hydrology Paper,* no. 3, 1964.

[9] M. T. van Genuchten, "A Closed-form Equation for Predicting the Hydraulic Conductivity of Unsaturated Soils," *Soil Sci. Soc. Am. J.,* vol. 44, pp. 892-898, September 1980.

[10] K. C. O. a. G. M. Pruess, "TOUGH2 User's Guide, Version 2.0," Report LBNL-43134, Lawrence Berkeley National Laborator, Berkeley, California, 1999.

[11] T. N. a. W. P. A. Narasimhan, "An integrated finite difference method for analyzing fluid flow in porous media," *Water Resour. Res,* vol. 12, no. 1, p. 57–64, February 1976.

[12] Sintef - MatMoRA project, "The Johansen Data Set," Sintef, 31 March 2009. [Online]. Available: http://www.sintef.no/Projectweb/MatMoRA/Downloads/Johansen/. [Accessed March 2013].

[13] G. Eigestad, H. K. Dahle, B. Hellevang, F. Riis, W. Johansen and Ø. E. Johansen, "Geological modeling and simulation of CO2 injection in the Johansen formation," *Computational Geosciences,* vol. 13, no. 4, pp. 435-450, December 2009.

[14] G. Bacci, "An Experimental and Numerical Investigation into Permeability and Injectivity Changes during CO2 Storage in Saline Aquifers," London, UK, 2011.

[15] Zhou Q, et al., "A method for quick assessment of CO2 storage capacity in closed and semi-closed saline formations," 2008. [Online]. Available: http://esd.lbl.gov/files/research/programs/gcs/projects/storage_resources/journal_3_NETL_zhou_etal_IJGGC.pdf.

[16] E.ON UK, *Basis of Design for Studies - Phase 1A,* E.ON UK, 2012.

[17] E-ON UK, *Vertical Flow performance,* E.ON UK, 2012.

[18] E.ON UK, Offshore & Transport System CO2 Process System Demo Phase (Base Case) Process Flow Diagram, 2010.

[19] E.ON UK, Heat & Mass Balance Demo Phase and Full Flow, 2010.